Available online at www.sciencedirect.com

ScienceDirect

Nuclear Physics A 1038 (2023) 122721

NUCLEAR PHYSICS A

www.elsevier.com/locate/nuclphysa

Temperature dependence of the static quark diffusion coefficient

Debasish Banerjee [a,b,*], Saumen Datta [c], Rajiv V. Gavai [d], Pushan Majumdar [e,1]

[a] *Saha Institute of Nuclear Physics, HBNI, Kolkata 700064, India*
[b] *Homi Bhabha National Institute, Training School Complex, Anushaktinagar, Mumbai 400094, India*
[c] *Tata Institute of Fundamental Research, Homi Bhabha Road, Mumbai 400005, India*
[d] *Indian Institute of Science Education and Research, Bhauri, Bhopal 462066, India*
[e] *Indian Association for the Cultivation of Science, Raja S. C. Mullick Road, Kolkata 700032, India*

Received 5 February 2023; received in revised form 5 July 2023; accepted 6 July 2023
Available online 13 July 2023

Abstract

The propagation of a low momentum heavy quark in a deconfined quark-gluon plasma can be understood in terms of a Langevin description. The momentum exchange with the plasma in thermal equilibrium can then be parametrized in terms of a single heavy quark momentum diffusion coefficient κ, which needs to be determined nonperturbatively. In this work, we study the temperature dependence of κ for a static quark in a gluonic plasma, with a particular emphasis on the temperature range of interest for heavy ion collision experiments.

Keywords: Heavy Quark Diffusion Constant; Quark gluon plasma; Lattice gauge theory; Spectral function; Heavy-ion collisions

* Corresponding author.
E-mail addresses: debasish.banerjee@saha.ac.in (D. Banerjee), saumen@theory.tifr.res.in (S. Datta), gavai@tifr.res.in (R.V. Gavai).
[1] Deceased.

https://doi.org/10.1016/j.nuclphysa.2023.122721
0375-9474/

1. Introduction

The charm and the bottom quarks provide very important probes of the medium created in the relativistic heavy ion collision experiments. Since the masses of both of these quarks are much larger than the temperatures attained in RHIC and in LHC, one expects these quarks to be produced largely in the early pre-equilibrated state of the collision. Heavy quark probes therefore provide a window to look into the early stages of the fireball.

In particular, the nature of the interaction of the heavy quarks with the thermalized medium is different from that of the light quarks. For energetic jets, radiative energy loss via bremsstrahlung is expected to be the dominant energy loss mechanism. For heavy quarks, the radiative energy loss is suppressed in a cone of angle $\sim m_Q/E$ [1]. For heavy quarks of moderate energy, $E \lesssim 2m_Q$, elastic collision with thermal quarks and gluons is expected to be the dominant mechanism of energy loss [2,3].

Even if the kinetic energy of the heavy quark is $\mathcal{O}(T)$, where T is the temperature of the fireball, its momentum will be much larger than the temperature. Its momentum is, therefore, changed very little in a single collision, and successive collisions can be treated as uncorrelated. Based on this picture, a Langevin description of the motion of the heavy quark in the medium has been proposed [4], [2,3]. v_2, the elliptic flow parameter, can then be calculated in terms of the diffusion coefficient of the heavy quark in the medium. The diffusion coefficient has been calculated in perturbation theory [2,4]. While this formalism works quite well in explaining the experimental data for R_{AA} and v_2 of the D mesons (see [5] for a review), the diffusion coefficient required to explain the data is found to be at least an order of magnitude lower than the leading order (LO) perturbation theory (PT) result.

This is not a surprise per se, as the quark-gluon plasma is known to be very nonperturbative at not-too-high temperatures, and various transport coefficients have been estimated to have values very different from LOPT. However, this makes it important to have a nonperturbative estimate of the heavy quark diffusion coefficient. A field theoretic definition of the heavy quark diffusion coefficient at zero momentum, κ, to leading order of an $1/M$ expansion, was given in [6,7]. The next-to-leading order (NLO) calculation of the diffusion coefficient in perturbation theory [8] was found to change the LO result by nearly an order of magnitude at temperatures $\lesssim 2T_c$. The large change from LO to NLO indicates an inadequacy of perturbation theory in obtaining a reliable estimate for the diffusion coefficient in the temperature range of interest, and makes a nonperturbative estimate essential.

The first nonperturbative results for κ, using the formalism of [7] and numerical lattice QCD in the quenched approximation (i.e., gluonic plasma), supported a value of κ substantially different from LOPT and in the correct ballpark for HIC phenomenology [9]. Of course, the plasma created in experiments is not a gluonic plasma; but the fact that the quenched QCD result is of the right order of magnitude gave strong support for the Langevin description of the heavy quark energy loss. A first lattice study with light (though somewhat unphysically heavy) quarks has recently been performed, and indicates a rather large effect of thermal quarks [10]. While the effects of thermal quarks need to be explored more, for proper understanding of various systematics of the calculation, and detailed analysis of the parametric behavior of κ, studies in quenched QCD are still important. Some of these issues were addressed in Refs. [11–13]. In particular, Refs. [11,13] conducted a study at 1.5 T_c, and explored various systematics in the numerical calculation of κ. The focus of Ref. [12] was a comparison with perturbation theory, and asymptotically high temperatures were explored. Meanwhile, a nonperturbative definition of the first correction to

the static limit was discussed in [14]. Nonperturbative estimates of this correction have recently been carried out [15,16].

In this work we have carried out a study of the static quark momentum diffusion coefficient κ in the temperature range $\lesssim 3.5T_c$, following the formalism of [7]. The focus here is on studying the temperature dependence of κ in the temperature range of interest for the relativistic heavy ion collision experiments. We extend the temperature range studied in [9] to cover the entire temperature range of interest to the heavy ion community, and also improve the analysis technique, following Refs. [11] and [15]. After explaining the formalism and our calculational techniques in Section 2 and Section 3, respectively, we present the results of our study in Section 4. Combined with the $1/M$ correction terms calculated in [15], we can get the results for momentum diffusion coefficients for the charm and the bottom in the plasma. We discuss these results in Section 5, where also results from phenomenological and other QCD based studies are discussed.

2. Langevin formalism and nonperturbative definition of the momentum diffusion coefficient κ

In this section, we outline the formalism underlying our study. We first define the Langevin formalism for the heavy quark energy loss, as described in [4], [2,3], and then give a nonperturbative definition of the diffusion coefficient, following [6,7].

The heavy quark momentum is much larger than the system temperature T: even for a near-thermalized heavy quark with kinetic energy $\sim T$, its momentum $p_Q \sim \sqrt{m_Q T}$, where m_Q is the heavy quark mass. Individual collisions with the medium constituents with energy $\sim T$ do not change the momentum of the heavy quark substantially if $m_Q \gg T$. Therefore, the motion of the heavy quark is similar to a Brownian motion, and the force on it can be written as the sum of a drag term and a "white noise", corresponding to uncorrelated random collisions:

$$\frac{dp_i}{dt} = -\eta_D\, p_i + \xi_i(t), \qquad \langle \xi_i(t)\xi_j(t')\rangle = \kappa\, \delta_{ij}\, \delta(t-t'). \tag{1}$$

In general, the force-force correlation will depend on the momentum of the heavy quark, and can be expressed in terms of two diffusion coefficients $\kappa_L(p)$ and $\kappa_T(p)$, corresponding to directions parallel and perpendicular to the momentum, respectively. As $p \to 0$, $\kappa_L(p),\ \kappa_T(p) \to \kappa$. The momentum diffusion coefficient, κ, can be obtained from the correlation of the force term:

$$\kappa = \frac{1}{3}\int_{-\infty}^{\infty} dt\, \sum_i \langle \xi_i(t)\, \xi_i(0)\rangle. \tag{2}$$

The drag coefficient, η_D, can be connected to the diffusion coefficient using standard fluctuation-dissipation relations [17]:

$$\eta_D = \frac{\kappa}{2m_Q T}. \tag{3}$$

In the leading order in an expansion in $\frac{1}{m_Q}$, the heavy quark interacts only with the color electric field of the plasma. Therefore the momentum diffusion coefficient κ can be obtained from the electric field correlation function [6,7]

$$G_{EE}(\tau) = -\frac{1}{3}\sum_{i=1}^{3} \frac{\left\langle \Re\,\mathrm{Tr}\,\left(U(L_\tau,\tau)\, gE_i(\tau,\vec{x})\, U(\tau,0)\, gE_j(0,\vec{x})\right)\right\rangle}{\langle \Re\,\mathrm{Tr}\, U(L_\tau,0)\rangle}\,. \tag{4}$$

Here $U(\tau_1, \tau_2)$ is the gauge link in Euclidean time from τ_1 to τ_2 at spatial coordinate $\vec{x}$, $E(\tau, \vec{x})$ is the color electric field insertion at Euclidean time τ, $L_\tau = 1/T$ is the length of the Euclidean time direction, $\langle ... \rangle$ indicates thermal averaging, and an average over the spatial coordinate $\vec{x}$ is implied (see [7] for a formal derivation).

The spectral function, $\rho_T(\omega)$, for the force term is connected to $G_{EE}(\tau)$ by the integral equation [17]

$$G_{EE}(\tau) \;=\; \int_0^\infty \frac{d\omega}{\pi}\, \rho_T(\omega)\, \frac{\cosh\omega(\tau - \frac{1}{2T})}{\sinh\frac{\omega}{2T}}\cdot \tag{5}$$

The momentum diffusion coefficient, κ_E, is then given by

$$\kappa_E \;=\; \lim_{\omega\to 0} \frac{2T}{\omega}\, \rho_T(\omega)\cdot \tag{6}$$

In this work we will use eq. (5), eq. (6) to calculate the momentum diffusion coefficient κ_E for moderately high temperatures $T \lesssim 3.5T_c$. In particular, we will be exploring the temperature dependence of κ_E/T^3.

Note that κ_E is the leading order estimate of κ in an $\frac{1}{m_Q}$ expansion. The $\mathcal{O}(m_Q^{-1})$ correction has been explored [14]: one can write [18]

$$\kappa \approx \kappa_E \;+\; \frac{2}{3}\,\langle v^2\rangle\, \kappa_B, \tag{7}$$

where $\langle v^2\rangle \;\approx\; \frac{3T}{M_{\rm kin}}$ is the thermal velocity squared, and $M_{\rm kin}$ is the kinetic mass, of the heavy quark. κ_B is the estimate of the diffusion coefficient one gets by replacing the electric fields with magnetic fields in eq. (5) and eq. (6). It has been calculated in Ref. [15] for the gluonic plasma.

3. Outline of the calculation

We calculated the electric field correlator $G_{EE}(\tau)$, eq. (4), for gluonic plasma using lattice discretization and numerical Monte Carlo techniques. On the lattice, the electric field was discretized, following [7], as

$$E_i(\vec{x}, \tau) \;=\; U_i(\vec{x}, \tau)\, U_4(\vec{x} + \hat{i}, \tau) \;-\; U_4(\vec{x}, \tau)\, U_i(\vec{x}, \tau + 1)\cdot$$

Then the lattice discretized EE correlator takes the form

$$G^{\rm bare}_{EE}(\tau) \;=\; \frac{1}{V}\sum_{\vec{x}} \frac{C^i(\tau+1, \vec{x}) + C^i(\tau-1, \vec{x}) - 2C^i(\tau, \vec{x})}{\prod_{x_4=0}^{L_\tau} U_4(\vec{x}, x_4)} \tag{8}$$

where $C^i(\tau, \vec{x})$ are Wilson lines at $\vec{x}$ with a hook of length τ in the i direction, i.e.,

$$C^i(\tau, \vec{x}) \;=\; U_i(\vec{x}, 0) \prod_{x_4=0}^{\tau-1} U_4(\vec{x} + \hat{i}, x_4)\, U_i^\dagger(\vec{x}, \tau) \prod_{x_4=\tau}^{L_\tau} U_4(\vec{x}, x_4)\cdot$$

We have calculated the correlators $G^{\rm bare}_{EE}$ on the lattice at various temperatures $\lesssim 3.5T_c$. Equilibrium configurations for a gluonic plasma were generated at various temperatures by using lattices with temporal extent $N_\tau = \frac{1}{T\, a(\beta)}$, where a is the lattice spacing, and $\beta = \frac{6}{g_B^2}$ is the

Table 1
Summary of runs and statistics.

β	N_τ	N_σ	T/T_c	# sublattice	# update	# conf
7.05	20	64	1.50	5	500	1270
7.192	24	72	1.48	4	2000	2032
7.30	20	64	2.03	5	500	1200
7.457	24	80	2.04	4	500	1000
	20	80	2.45	6	500	730
7.634	30	96	2.01	5	2000	640
	24	96	2.51	4	2000	657
	20	96	3.01	5	2000	500
7.78	28	96	2.55	7	2000	678
	24	96	2.98	4	2000	536
	20	96	3.55	5	2000	522
7.909	28	96	2.96	7	2000	1100
	24	96	3.46	6	2000	967

coefficient of the plaquette term in the Wilson gauge action. The details of the lattices generated and the number of configurations at each parameter set is given in Table 1.

The spatial extent of the lattices are chosen such that $LT > 3$ and also the lattice is confined in the spatial direction. At various temperatures we have more than one lattice spacings; this allows us to estimate the discretization error, and to get the continuum result. Also for various values of the coupling, we have changed N_τ to change the temperature, keeping all the other parameters of the lattice unchanged. A comparison of the results from such lattices give us a direct handle on the temperature modification of κ_E.

Since we require very accurate correlation functions on lattices with large temporal extents, we have used the multilevel algorithm [19] in calculating eq. (8). We follow the implementation of the algorithm outlined in [9]. The number of sublattices for the multilevel update, and the number of sublattice updates, are shown in Table 1, where each update consisted of (1 heatbath+3 overrelaxation) steps. Typically, a few parallel streams with independent random number seeds were used at each parameter sets. After a thermalization run which is many times the autocorrelation length, $\mathcal{O}(10^2 - 10^3)$ configurations were generated from each stream. The total number of configurations generated at each parameter set is shown in Table 1.

The temperature scale shown in Table 1 is obtained from the interpolation formula [20]

$$\log \frac{r_0}{a} = \left[\frac{\beta}{12\, b_0} + \frac{b_1}{2\, b_0^2} \log \frac{6 b_0}{\beta} \right] \frac{1 + c_1/\beta + c_2/\beta^2}{1 + c_3/\beta + c_4/\beta^2} \tag{9}$$

where $b_0 = 11/(4\pi)^2$ and $b_1 = 102/(4\pi)^4$. The fit parameters c_i are

$$c_{\{1,2,3,4\}} = \{-8.9664,\ 19.21,\ -5.25217,\ 0.606828\} \tag{10}$$

and $r_0 T_c = 0.7457$ [20]. Other ways of determining the temperature gives slightly different values: e.g., using the formula of Ref. [21] leads to a temperature which differs by $\sim$ 1-1.5% at the higher β values of Table 1. So we will effectively round off the temperature and, e.g., treat 3.46 T_c and 3.55 T_c in Table 1 as $\sim 3.5 T_c$. The physical value of T_c for the gluonic plasma also depends somewhat on how the scale is set. Using the value of $r_0 T_c$ quoted above, and taking $r_0 \approx$ 0.5 fm [22] one gets $T_c \approx 294$ MeV.

4. Analysis of the correlators and extraction of κ/T^3

4.1. Discretization effect in $G_{EE}^{\rm bare}$

The EE correlation functions $G_{EE}(\tau)$ are ultraviolet finite. The bare correlators $G_{EE}^{\rm bare}(\tau)$ require only finite renormalization:

$$G_{EE}^{\rm renorm}(\tau) \;=\; Z_{EE}(a(\beta))\, G_{EE}^{\rm bare}(\tau)\,. \tag{11}$$

The renormalization coefficient $Z_{EE}(a)$ has been determined at one loop level in [23]:

$$Z_{EE} \;=\; 1 \,+\, \frac{2 g_B^2 C_f}{3}\, P_1 \;\approx\; 1 \,+\, 0.1377\, g_B^2 \tag{12}$$

where the lattice bare coupling $g_B^2 = \frac{6}{\beta}$, $C_f = \frac{4}{3}$, and $P_1 = \int_{-\pi}^{\pi} \frac{d^4k}{(2\pi)^4}\, \frac{1}{K^2} \approx 0.15493$.

The renormalization constant needed here, eq. (11), is a finite renormalization constant that is expected to go to 1 on taking the continuum limit. However, it is known that this approach is slow [24], and an accurate estimation of Z_{EE} is important for a proper estimation of the continuum limit. Unfortunately, for Z_{EE} only the one loop result is available. We can make a guesstimate of the uncertainty involved by doing a mean field-like treatment of the renormalization factor: handling the large renormalization of the gauge links through nonperturbative information of the plaquette variable [24]. This leads to a tadpole-corrected renormalization factor

$$Z_{EE}^{\rm tad} \;\approx\; \frac{1 \,+\, \left(0.1377 \,-\, \frac{1}{3}\right) g_B^2}{\langle P(\beta)\rangle} \tag{13}$$

where $\langle P(\beta)\rangle$ is the vacuum expectation value of the spacetime averaged plaquette variable $P = \langle \frac{1}{3}\,\mathrm{Tr}\, \prod_{l\in\square} U_l \rangle$.

For our values of the coupling, $Z_{EE}^{\rm tad}$ differ from Z_{EE} by $\sim 7-9\%$ on individual lattices, and the continuum extrapolated correlators differ by $\lesssim 7\%$. For the value of the diffusion coefficient κ, we checked that the variation in the estimate, due to normalization by $Z_{EE}^{\rm tad}$, is comfortably within the spread due to other systematics quoted in Section 4.2 (dominated by the uncertainty in the fit form).

After the renormalization, the correlator still shows cutoff effect, especially at short distances. A major part of this cutoff effect at short distances can be taken into account by a consideration of the discretization effect in the leading order. In leading order, the EE correlator takes the form [25]

$$G_{EE}(\tau, LO) = g^2\, C_f\, G_{norm}(\tau), \tag{14}$$

$$G_{\rm norm}^{\rm Cont}(\tau) = \pi^2 T^4\, \mathrm{cosec}^2(\pi\tau T)\, \left(\cot^2(\pi\tau T) \,+\, \frac{1}{3}\right) \tag{15}$$

$$G_{\rm norm}^{\rm Lat}(\tau) = \frac{1}{3a^4} \int \frac{d^3k}{8\pi^3}\, \frac{e^{\bar{k}(N_\tau - t)} + e^{\bar{k}t}}{e^{\bar{k}N_\tau} \,-\, 1}\, \frac{\tilde{k}^2}{\sinh\bar{k}} \tag{16}$$

where the integration is over the Brillouin zone $(-\pi, \pi)$ and

$$\frac{\bar{k}}{2} \;=\; \mathrm{arcsinh}\, \frac{\tilde{k}}{2}\,, \qquad \tilde{k}^2 \;=\; \sum_{i=1}^{3} 4\, \sin^2 \frac{k_i}{2}\,. \tag{17}$$

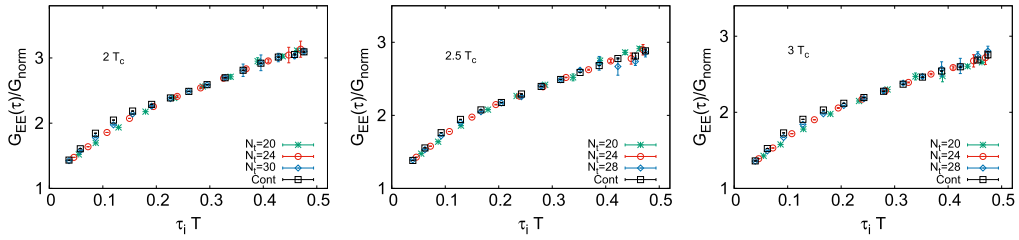

Fig. 1. Continuum extrapolation of the correlator ratio $\frac{G_{EE}}{G^{\rm Lat}_{\rm norm}}(\tau)$, at (left) 2 T_c, (middle) 2.5 T_c, and (right) 3 T_c.

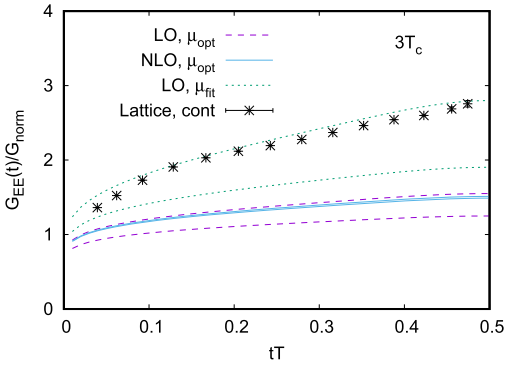

Fig. 2. A comparison of the nonperturbatively obtained correlator $\frac{G_{EE}}{G^{\rm Lat}_{\rm norm}}(\tau)$ at $T = 3T_c$ with the results of perturbation theory [27]. The LO and NLO results use an optimized scale (eq. (19)). Also shown is the LO result with the scale $\mu_{\rm fit}$ (eq. (20)). In each case, the bands for the perturbation theory are obtained by varying the scale by a factor of two in each direction from the scale mentioned above.

A major part of the discretization effect can be accounted for by a comparison of eq. (15) with eq. (16): in particular, by defining an improved distance $\tau_{\rm imp}$ through [22,25]

$$G^{\rm Lat}_{\rm norm}(\tau_{\rm imp}) \;=\; G^{\rm Cont}_{\rm norm}(\tau)\,. \tag{18}$$

We have $G^{\rm bare}_{EE}(\tau)$ at multiple lattice spacings at each temperature. As noted in [11,12] before, we found that the use of $\tau_{\rm imp}$, eq. (18), reduces considerably the short distance discretization effect in $G_{EE}(\tau)$. In what follows, we have used $\tau_{\rm imp}$ to denote the distance scale for $G^{\rm renorm}_{EE}$.

At $T/T_c = 2$, 2.5 and 3 we have three lattice spacings each. Using these correlators, we find the continuum extrapolated correlators at distances corresponding to $\tau_{\rm imp}$ for the finest lattice. We extrapolate $\frac{G_{EE}}{G^{\rm Lat}_{\rm norm}}(\tau)$ to $a \to 0$, where τ takes the values $\tau_{\rm imp}$ of the finest lattice at each temperature. The details of the method are presented in Appendix A. The correlators $\frac{G_{EE}}{G^{\rm Lat}_{\rm norm}}(\tau)$ for the different discretized lattices, and their continuum extrapolated value, are shown in Fig. 1. The extrapolated ratio is now multiplied by $G^{\rm Cont}_{\rm norm}(\tau)$ to get the continuum extrapolated correlator. The calculation is done through a bootstrap analysis [26]. The particulars of our bootstrap implementation are given in Appendix A.

It is interesting to compare the continuum extrapolated correlator with perturbation theory. G_{EE} has been calculated in perturbation theory to NLO in Ref. [27]; in Fig. 2 we compare

the perturbative results of Ref. [27] with our nonperturbatively determined correlator [28]. In Ref. [27] the scale for the running coupling has been set at

$$\mu_{\rm opt} \approx \max\left[7.57\,\omega,\ 6.74\,T\right] \tag{19}$$

following the principle of minimal sensitivity. The LO and NLO bands in Fig. 2 are obtained by varying $\mu \in [0.5, 2]\,\mu_{\rm opt}$. This way of scale setting leads to a good agreement between the LO and the NLO calculation; but as Fig. 2 shows, the perturbative estimates are very different from the nonperturbative results. We also show the LO results obtained by setting the scale in an intuitive way [11]:

$$\mu_{\rm fit} = \max\left[\omega, \pi T\right]\cdot \tag{20}$$

The band is obtained by varying this scale by a factor [0.5, 2.0] as before. As Fig. 2 shows, the LO curve captures the main features of the nonperturbative result. However, the good agreement of perturbation theory with the lattice result in this case is misleading, as the NLO result changes strongly from the LO result and the lattice result. Guided by Fig. 2, we will use the LO spectral function evaluated at the scale $\mu_{\rm fit}$ for modeling the ultraviolet part of the spectral function.

4.2. Extraction of κ from the correlators

A direct inversion of eq. (5) to get $\rho_T(\omega)$ is very difficult. Instead, to get an estimate of what kind of κ_E is consistent with the G_{EE} obtained, we have used some simple models for $\rho_T(\omega)$. Our models, and the analysis strategy, are similar to what was followed in Ref. [15] for $G_{BB}(\tau)$, which, in turn, was influenced by earlier works [9,11] on $G_{EE}(\tau)$. The ultraviolet and the infrared parts of $\rho_T(\omega)$ are modeled with the simple forms

$$\rho_{UV}(\omega) = \frac{g^2(\mu_{\rm fit})\,C_f\,\omega^3}{6\pi}, \qquad \rho_{IR}(\omega) = \frac{\kappa_E\,\omega}{2T}, \tag{21}$$

where $\mu_{\rm fit}$ is defined in eq. (20). $\rho_{IR}(\omega)$ is the simplest form capturing the dissipative behavior of κ_E. The correlator eq. (4) does not have a transport peak, and is expected to have a smooth linear behavior in the infrared [7,27,29], motivating $\rho_{IR}(\omega)$ [30]. $\rho_{UV}(\omega)$ is the known leading order form of the spectral function and the scale choice is motivated by Fig. 2. The NLO spectral function is known [27] but, as Fig. 2 shows, it is not clear that it will capture the ultraviolet behavior better except at very high ω.

While both $\rho_{UV}(\omega)$ and $\rho_{IR}(\omega)$ are well-motivated, not much is known a-priori about the form of the spectral function in the intermediate ω regime. An ansatz, that allows $\rho_T(\omega)$ to continuously change from $\rho_{UV}(\omega)$ to $\rho_{IR}(\omega)$, is

$$\rho_T(\omega) = \max\left[c\,\rho_{UV}(\omega),\ \rho_{IR}(\omega)\right] \tag{22}$$

where we have introduced a parameter c to take into account the uncertainty due to the scale choice and the use of the leading order form for $\rho_{UV}(\omega)$. c is treated as a fit parameter. The best fit values we obtained for c are close to 1, in the range 1-1.2.

A more smooth form of connecting $\rho_{UV}(\omega)$ with $\rho_{IR}(\omega)$ is

$$\rho_T(\omega) = \left[\sqrt{(c\,\rho_{UV}(\omega))^2 + \rho_{IR}(\omega)^2}\right]\cdot \tag{23}$$

The form of eq. (23) has been argued to be theoretically better justified in [11], [13]. Here again, the fit parameter $c \sim 1$ is introduced to account for the uncertainty in $\rho_{UV}(\omega)$. In our analysis we have treated eq. (22) and eq. (23) at par.

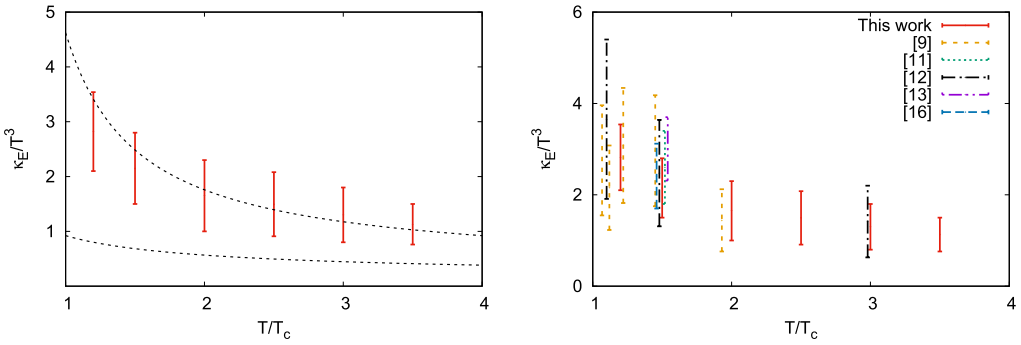

Fig. 3. (Left) Our estimates for the range of κ_E/T^3 in the temperature range $\lesssim 3.5T_c$. Also shown (dotted lines) is the NLO perturbation theory estimate eq. (26) [8]; the band corresponds to varying the scale of the coupling $g^2(\mu)$ in the range $\mu \in [\pi T, 4\pi T]$. (Right) A survey of other existing lattice results for κ_E in gluonic plasma in the 1-4 T_c temperature range. For visual clarity, points at 1.5 T_c and 3 T_c have been slightly shifted horizontally.

Table 2
Temperature dependence of κ_E/T^3.

T/T_c	1.2	1.5	2.0	2.5	3.0	3.5
κ_E/T^3	2.1 - 3.5	1.5 - 2.8	1.0 - 2.3	0.9 - 2.1	0.8 - 1.8	0.75 - 1.5

Instead of introducing a fit parameter c as above, ref. [11] has suggested parametrizing the difference between the above forms (with c=1) and $\rho_T(\omega)$ in a sine expansion:

$$\left(1 + \sum_n c_n \sin(\pi n y)\right), \qquad y = \frac{x}{1+x}, \quad x = \log\left(1 + \frac{\omega}{\pi T}\right).$$

For the fit range we used, we found that one term in the expansion sufficed to fit our correlator. Therefore we have also tried the fit forms

$$\rho_T(\omega) = (1 + c_1 \sin \pi y) \left[\sqrt{\rho_{UV}(\omega)^2 + \rho_{IR}(\omega)^2}\right]; \tag{24}$$

$$= (1 + c_1 \sin \pi y) \max\left[\rho_{UV}(\omega), \rho_{IR}(\omega)\right]. \tag{25}$$

In all our fits we have found c_1 to be small, $\in [0.02, 0.12]$.

We perform the whole analysis for each of the model forms eq. (22), eq. (23), eq. (24) and eq. (25) in a bootstrap framework. Our final estimates of κ_E are shown in Table 2 and in Fig. 3. The details of the analysis can be found in Appendix A, where the estimates for each model are given in Table 3 and Fig. 7. Our estimates in Table 2 and Fig. 3 include the entire bands for eq. (23), eq. (22) and the central values for eq. (24), eq. (25).

There are other estimates of κ_E/T^3 for a gluonic plasma from the lattice. While Ref. [9] studied the temperature range close to T_c, a detailed study at 1.5 T_c was performed in Ref. [11]. A broad temperature range was studied in Ref. [12], with the main focus being very high temperatures. While the analysis techniques, in particular the spectral function models, vary, all these references used the multilevel algorithm and perturbative renormalization constants. Recently, Refs. [13] and [16] have used gradient flow [31] to get the renormalized EE correlators at 1.5 T_c. We compare these studies with ours in the right panel of Fig. 3. Within the uncertainties of our and other studies, our results agree very well with these other quenched lattice studies.

5. Discussion of the results

Let us see how the temperature dependence of κ_E, obtained in Section 4.2, compares with perturbation theory. κ_E/T^3 has been calculated to NLO in perturbation theory in [8]. For SU(3) gluonic plasma, the NLO result is

$$\kappa_E/T^3 \;=\; \frac{g^4 C_F}{6\pi}\, T^3 \left[\log\frac{2T}{m_D} \;+\; \xi \;+\; C\, g\right] \tag{26}$$

where $C_F = 4/3$, $\xi \approx -0.64718$, $C \approx 2.3302$ and $m_D = gT$ in LO perturbation theory. This NLO result is shown in Fig. 3 by the band bordered by the dotted lines; the band corresponds to evaluating g^2 at the scales $\mu \in [\pi T, 4\pi T]$. The NLO results explain the data quite well. Note, however, that perturbation theory is inherently unstable here: the LO result is an order of magnitude smaller than NLO. In fact, if we omit the $\mathcal{O}(g)$ term in eq. (26), we will get a negative value for κ_E/T^3 in our temperature range [27].

There have been various QCD-based estimates of κ that incorporate some nonperturbative effects. In particular, in the T-matrix approach [32] the interaction between various partons and heavy quarks are taken into account by trial potentials as input to the T matrix, which are then tuned to reproduce the equation of state and the quarkonia correlators. In more phenomenological quasiparticle approaches, the thermal masses of quarks and gluons and the coupling strength are fitted. We will discuss some of these results below Fig. 5.

It is of interest to compare our results on the temperature dependence of κ_E with some other, related theories. The estimate in Ref. [6] is for $\mathcal{N} = 4$ supersymmetric Yang-Mills theory, which is scale invariant. Clearly, κ_E/T^3 is temperature independent in such a theory. A different AdS-CFT based approach has been taken in Ref. [33], where the drag term has been connected to the spatial string tension, σ_s. Eqn. (3) then connects κ_E to σ_s. While the estimate of κ_E/T^3 obtained in Ref. [33] this way is close to our estimates, it provides a somewhat milder temperature dependence at higher temperatures.

While it is the momentum diffusion coefficient that enters the equations of Langevin dynamics and is of interest for the phenomenology of heavy quark thermalization, it has been the convention to quote the transport coefficient as the position space diffusion coefficient D_s. In particular, the combination

$$2\pi\, T\, D_s \;=\; \frac{4\pi}{\kappa/T^3} \tag{27}$$

is usually quoted. In the left panel of Fig. 4 we plot $2\pi\, T\, D_s$ as obtained form our results of κ_E using eq. (27).

For phenomenological studies, one is interested in estimates of κ for charm and bottom, rather than for the infinitely massive quarks. Using eq. (7) [14] one can provide such an estimate [15]. In Fig. 5 we show the separate estimates for D_s^c and D_s^b, obtained using eq. (7) and eq. (27), and the κ_E values of Table 2. The estimates of κ_B are from ref. [15], supplemented by a calculation at 3 T_c, following exactly the same analysis techniques as in Ref. [15]. The estimates we get for D_s^c and D_s^b are shown in Fig. 5. The details can be found in Appendix A.

$2\pi\, T\, D_s^{c,b}$ show a rising trend with temperature. The temperature dependence of D_s^c is of great interest to phenomenological studies [34–38]. In particular, in Ref. [37], using a parametric temperature dependence

$$2\pi\, T\, D_s \sim \alpha \;+\; \gamma\, \left(\frac{T}{T_c} - 1\right), \tag{28}$$

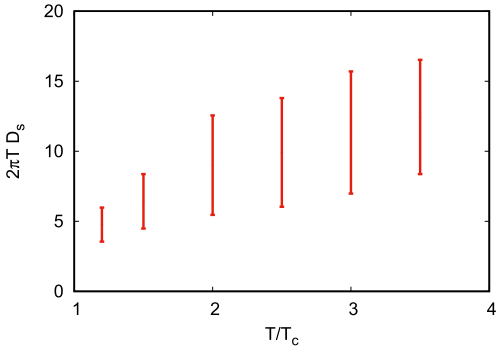

Fig. 4. An estimation of the static quark diffusion coefficient, using eq. (27) and Table 2.

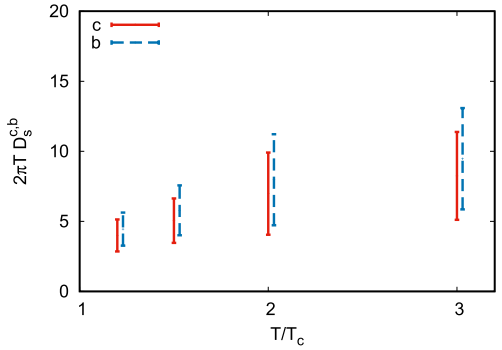

Fig. 5. Estimate of D_s^c and D_s^b, the spatial diffusion coefficients for the charm and bottom quarks, using eq. (7) and eq. (27). See text, and Table 5 in the appendix. For visual clarity, the points for D_s^b have been slightly shifted horizontally.

$2\pi\ T\ D_s$ was estimated from the experimental data for D meson using a Bayesian analysis. They quote the central values $(\alpha,\ \gamma) \sim (1.9,\ 3.0)$, with $\alpha \sim 1 - 3$ being the $5 - 95$ percentile band [37]. While our study is for quenched QCD, it is still interesting to check if the temperature dependences of D_s^c and D_s^b shown in Fig. 5 are consistent with the simple parametrization of eq. (28). The answer is "yes" (admittedly, aided by the large uncertainties in our measurements), with $(\alpha,\ \gamma) = (3.61(30),\ 2.57(43))$ for charm and $(3.99(35),\ 3.08(54))$ for bottom, respectively [39]. The ALICE collaboration's survey of phenomenological studies of D meson R_{AA} and flow quotes the range $1.5 < 2\pi T D_s < 4.5$ at T_c [34]; our value of α for charm is also consistent with this. For the static D_s, using the same parametrization (eq. (28)) we obtained $\alpha = 4.27(29)$ and $\gamma = 3.60(33)$. We also tried doing this linear fit for $2\pi\ T\ D_s$ from each of the models of Section 4.2. The results can be seen in Fig. 8 and Table 4 in Appendix A. All of the model spectral functions indicate a positive slope of $2\pi\ T\ D_s$ with temperature.

We emphasize that eq. (28) is a purely phenomenological fit: the temperature dependence of D_s is, of course, more complicated in general. We have already discussed the dependence in perturbation theory. The temperature dependence obtained in various QCD based studies that model the nonperturbative aspects in some way are discussed in [35]; the behavior obtained in some of them is very similar to Fig. 5. To mention a couple: in the T matrix approach, one gets two different sets of solutions. The solution with a "strong" potential, that includes a screened string term, leads to values and temperature dependence of D_s^c in very good agreement with Fig. 5,

while the scenario with a potential close to the free energy gives results which are somewhat different. Quasiparticle models can also give a similar temperature dependence to the behavior seen by us [38].

6. Summary

In this paper we have studied the electric field correlator, eq. (4), in a thermally equilibrated gluonic plasma at moderately high temperatures $T \lesssim 3.5T_c$, nonperturbatively using lattice QCD. We investigated in detail the cutoff dependence of the correlators (Fig. 1). With a simple set of models for the EE spectral function $\rho_T(\omega)$, we then estimated the static quark momentum diffusion coefficient κ_E.

κ_E and its temperature dependence for the gluonic plasma at moderately high temperatures are shown in Fig. 3 and in Table 2. Using eq. (7) and the results of [15] one can then calculate the diffusion coefficients for the charm and bottom quarks. These results are shown in Fig. 5 where, using standard practice, we have used eq. (27) to present the results for the diffusion coefficients $2\pi\ T\ D_s^{c,b}$.

The results presented here are for a gluonic plasma; first unquenched studies of κ_E (with unphysically heavy pion) indicate that the effects of thermal quarks can be large [10]. It is still interesting to compare our results for D_s^c and its temperature dependence with the phenomenological studies. In Section 5 we compare our results to some QCD-based model studies and also to phenomenological extractions of D_s^c from the experimental data [34,37], and find very good agreement.

CRediT authorship contribution statement

Debasish Banerjee: Conceptualization, Writing – review & editing. **Saumen Datta:** Conceptualization, Formal analysis, Methodology, Software, Writing – original draft. **Rajiv V. Gavai:** Conceptualization, Writing – review & editing. **Pushan Majumdar:** Conceptualization, Methodology, Software.

Declaration of competing interest

The authors declare the following financial interests/personal relationships which may be considered as potential competing interests: The Authors declare that the decision of submission to this journal is based on the open access feature of the journal and the subject relevance. The Authors are aware that the co-author RVG is on the Editorial Board, but the decision to submit to this journal has not been influenced by this fact.

Data availability

Data will be made available on request.

Acknowledgements

We thank Mikko Laine for providing the perturbative curves in Fig. 2 and for discussions. We also thank Santosh Das for discussions. The computations presented in this paper were performed on the clusters of the Department of Theoretical Physics, TIFR, and on the ILGTI computing

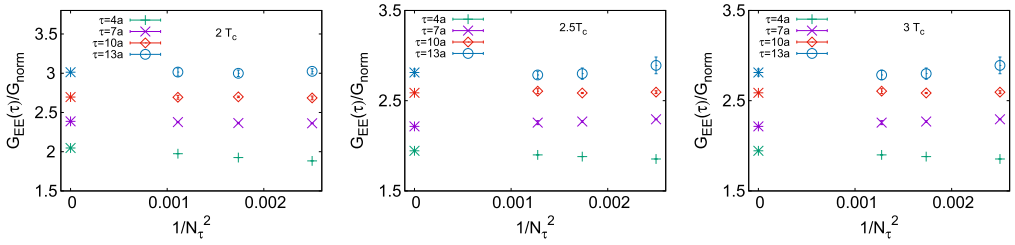

Fig. 6. Illustration of the continuum extrapolation of the correlator normalized by G_{norm}. (Left) 2 T_c, (middle) 2.5 T_c and (right) 3 T_c.

facilities of IACS and TIFR. We would like to thank Ajay Salve and Kapil Ghadiali for technical assistance. S.D. and R.V.G. acknowledge the support of the Department of Atomic Energy, Government of India, under Project Identification No. RTI 4002 and Raja Ramanna Fellowship respectively.

Appendix A. Some details of the numerical analysis

Here we provide additional details of our numerical analysis in Section 4.

We do a detailed calculation at temperatures $T/T_c = 2$, 2.5 and 3. At these temperatures we have correlators from three lattice spacings. We have estimated the continuum correlator from them, and calculated κ_E. Our whole analysis is done within a bootstrap formalism [26]. For the bootstrap analysis, the data of each set s is first blocked into N_s blocks, with blocksize at least 2-3 times the autocorrelation length. Now N_b bootstrap samples are created from each set by randomly choosing N_b blocks with replacement. For each bootstrap sample now the continuum correlator is obtained by the continuum extrapolation of the correlators.

The correlators for the sets at different lattice spacings are measured at different distances. For the continuum extrapolation, the correlators are interpolated to get the correlation functions at distances corresponding to the $\tau_{\rm imp}$ values of the finest lattice. We use a weighted B-spline of order 3 [40] for the interpolation, where the correlator data at each point is weighted by the standard error calculated for the bootstrap sample, and is fitted by a combination of spline functions. For the error estimation of the continuum correlator, a bootstrap analysis is done within each bootstrap sample.

Note that the continuum extrapolation typically involves an extrapolation of the coarser sets at the smallest distance, but this is not a concern as this distance is not used in the fits. A very slight extrapolation is also required at the largest ($\tau \sim 1/2T$) distance point, but it is a very small extrapolation and we do not expect this to be a problem.

At short distances $\tau_{\rm imp}T \lesssim 0.15$ we see a clear discretization effect, which is approximately linear in a^2; we fit to a linear form to get the continuum correlator. For larger distances $\tau_{\rm imp}T > 0.25$ the correlators do not show a clear discretization effect. In particular, for correlators at large distances $\tau_{\rm imp}T \gtrsim 0.3$ we found a constant fit to be more reasonable. We show examples of our continuum extrapolation at some representative distances in Fig. 6. Note that we have also carried out the analysis with linear extrapolation at all distances; the κ values obtained agree within errorbar.

To extract κ_E from the continuum correlators using eq. (5), we have used the fit forms discussed in Section 4.2, and done a standard χ^2 fit. For the minimization and the B-spline fitting, scipy routines [41] were used. For the final estimate of κ of each fit form, the median of the

Table 3
Results for κ_E/T^3 from the different fit forms of Section 4.2.

T/T_c	eq. (22)	eq. (23)	eq. (25)	eq. (24)
1.2	2.16-2.80	2.44-3.54	1.80-2.50	2.34-3.14
1.5	1.74-2.16	1.62-2.80	1.25-1.73	1.55-2.27
2	1.05-1.60	1.48-2.30	0.77-1.42	1.04-1.82
2.5	0.91-1.77	1.17-2.08	0.70-1.59	0.97-1.86
3	0.87-1.48	1.04-1.80	0.60-1.30	0.83-1.56
3.5	0.76-1.14	1.01-1.50	0.62-1.02	0.96-1.33

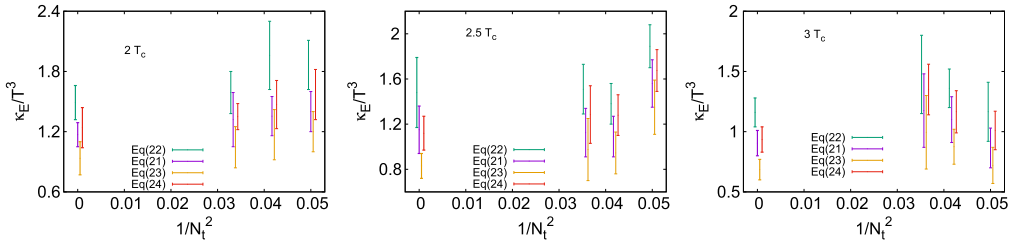

Fig. 7. Results for κ_E/T^3 obtained at $T/T_c = 2$ (left), 2.5 (middle) and 3 (right). Besides the continuum results, the results obtained from fitting individual lattices are also shown. See the text for details of the error band. (For interpretation of the colors in the figure(s), the reader is referred to the web version of this article.)

distribution of the bootstrap estimates is taken, and the $\mp 1\sigma$ band is obtained from the central 68% interval, i.e., from the [16,84] percentiles of the distribution. The results for the various fit forms are shown in Fig. 7. Typically we get a good χ^2 by taking the whole range except the two shortest distance points. We have, however, also varied $\tau_{\rm imp}^{\rm min}$. The results shown in Fig. 7 include the variation with fit range, and any difference due to using linear vs constant extrapolation at large separations in Fig. 6.

As mentioned in Section 4.2, we have also fitted the correlators from the individual lattices to the forms of Section 4.2. For this we have used $\tau_{\rm imp}^{\rm min} \sim 0.25/T$, where the discretization effect on the correlators is small. $\tau_{\rm imp}^{\rm min}$ is further varied within a small range. The bands shown in Fig. 7 include the spread due to such a variation.

In Table 3 we show the final results for κ_E/T^3 using the different fit forms. The error estimate is conservative, covering the 1σ interval obtained from the continuum correlator and the correlators from lattices with $N_t \geq 24$.

Table 3 also includes two temperatures where we have only two lattice spacings each, and 1.2 T_c where we have reanalyzed the correlators on N_t=24 lattices calculated in Ref. [15]. In these cases we have only fitted the individual lattices. The rest of the discussion is the same as above. The final result in these cases is taken from the N_t=24 lattices.

For the final result for κ_E shown in Fig. 3, we have treated the fit forms eq. (22) and eq. (23) at par, and conservatively quoted an error band that includes the bands for eq. (22) and eq. (23) in Table 3 and the central values of the bands for eq. (22) and eq. (23). These results are also shown in Table 2.

Using Table 3 and eq. (27) we can also make separate estimates for $2\pi\ T\ D_s$ for each form of the model $\rho_T(\omega)$ in Section 4.2. This is shown in Fig. 8. The linearly rising behavior of each of

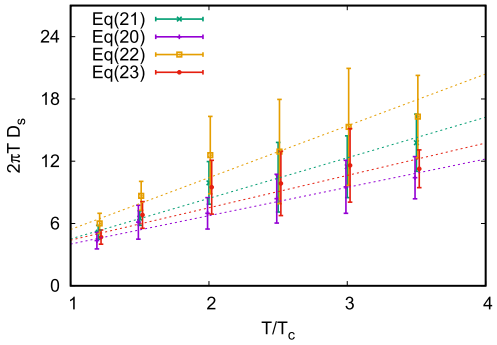

Fig. 8. An estimation of the static quark diffusion coefficient, using eq. (27) and Table 2. Also shown are the best fits to a linear temperature dependence (eq. (28)).

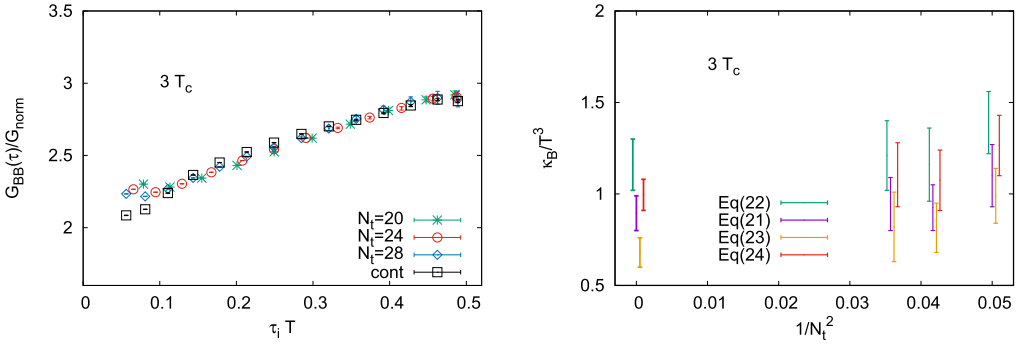

Fig. 9. (Left) The correlator $G_{BB}(\tau)$ at 3 T_c calculated at different lattice spacings, normalized by $G_{norm} = \frac{G_{BB}(\tau, LO)}{g^2 C_f}$. Also shown is the continuum extrapolated correlator. (Right) Estimates of κ_B/T^3 at 3 T_c obtained using the different fit forms. See text for explanation.

Table 4
The fit parameters for eq. (28).

	eq. (23)	eq. (22)	eq. (24)	eq. (25)
α	4.01(24)	4.51(27)	5.42(50)	4.39(45)
γ	3.91(39)	2.73(24)	4.99(71)	3.12(50)

these forms can then be separately fitted to the linear fit form eq. (28). The results of such a fit are shown in Table 4.

In Fig. 5 we show the estimates for D_s^c and D_s^b in the temperature range 1.2-3 T_c, using eq. (27), where κ^c and κ^b are obtained using eq. (7). The estimates for κ_B are taken from Ref. [15], supplemented with a calculation at 3 T_c. The BB correlator $G_{BB}(\tau)$ at 3 T_c at different lattice spacings, normalized by the corresponding leading order correlator $\frac{G_{BB}(\tau, LO)}{g^2 C_f}$ for lattice with the same N_τ, are shown in Fig. 9. We also show the corresponding continuum extrapolated correlator in the figure. The analysis for κ_B at 3 T_c follows that used in [15]; it is similar to the analysis for κ_E outlined in Section 3, except, following Ref. [15], the scale for the perturbative part of the BB spectral function is taken to be $\mu_{\rm fit}^B = \max\left[\omega^{\frac{5}{11}} (\pi T)^{\frac{6}{11}}, \pi T\right]$

Table 5
The estimates for $2\pi\ T\ D_s^{c,b}$, from eq. (27) and eq. (7).

	1.2 T_c	1.5 T_c	2 T_c	3 T_c
$2\pi\ T\ D_s^c$	2.9 - 5.1	3.5 - 6.6	4.0 - 9.9	5.1 - 11.4
$2\pi\ T\ D_s^b$	3.3 - 5.6	4.0 - 7.6	4.7 - 11.2	5.9 - 13.1

instead of eq. (20). The results obtained for κ_B for the different fit forms are also shown in Fig. 9. Taking a band that includes the different fit forms, we obtain an estimate $\kappa_B/T^3 \sim 0.6$ - 1.3 at 3 T_c.

Following Ref. [15], $\langle v^2 \rangle$ was estimated from a ratio of the susceptibilities calculated in [42]. This gives $\langle v^2 \rangle \approx (0.76, 0.40)$ for charm and bottom at 3 T_c, respectively (the values at the lower temperatures are given in Ref. [15]). At such temperatures, a nonrelativistic treatment of charm may be questionable. We find that the $\mathcal{O}(m_Q^{-1})$ corrections to κ, eq. (7), are $\sim 38\%$ for charm and $\sim 20\%$ for bottom.

From the results for κ^c and κ^b, D_s^c and D_s^b can be obtained using eq. (27). Since the range for κ is dominated by systematics, we simply find the range of D_s by using eq. (27) for the lower and upper bound of the range for κ. The results for $2\pi\ T\ D_s^{c,b}$ obtained this way are given in Table 5 and shown in Fig. 5.

References

[1] Y. Dokshitzer, D. Kharzeev, Phys. Lett. B 519 (2001) 199.
[2] G.D. Moore, D. Teaney, Phys. Rev. C 71 (2005) 064904.
[3] M.G. Mustafa, Phys. Rev. C 72 (2005) 014905.
[4] B. Svetitsky, Phys. Rev. D 37 (1988) 2484.
[5] X. Dong, Y-J. Lee, R. Rapp, Annu. Rev. Nucl. Part. Sci. 69 (2019) 417.
[6] J. Casalderrey-Solana, D. Teaney, Phys. Rev. D 74 (2006) 085012.
[7] S. Caron-Huot, M. Laine, G. Moore, J. High Energy Phys. 04 (2009) 053, arXiv:0901.1195.
[8] S. Caron-Huot, G. Moore, J. High Energy Phys. 0802 (2008) 081.
[9] D. Banerjee, S. Datta, R. Gavai, P. Majumdar, Phys. Rev. D 85 (2012) 014510, arXiv:1109.5738.
[10] L. Altenkort, et al., Phys. Rev. Lett. 130 (2023) 231902, arXiv:2302.08501.
[11] A. Francis, O. Kaczmarek, M. Laine, T. Neuhaus, H. Ohno, Phys. Rev. D 92 (2015) 116003.
[12] N. Brambilla, V. Leino, P. Petreczky, A. Vairo, Phys. Rev. D 102 (2020) 074503.
[13] L. Altenkort, A. Eller, O. Kaczmarek, L. Mazur, G. Moore, H.-T. Shu, Phys. Rev. D 103 (2021) 014511.
[14] A. Bouttefeux, M. Laine, J. High Energy Phys. 12 (2020) 150.
[15] D. Banerjee, S. Datta, M. Laine, J. High Energy Phys. 08 (2022) 128, arXiv:2204.14075.
[16] N. Brambilla, V. Leino, J. Mayer-Steudte, P. Petreczky, arXiv:2206.02861.
[17] J. Kapusta, C. Gale, Finite Temperature Field Theory: Principles and Applications, 2nd edition, Cambridge University Press, 2006.
[18] The analysis of [14] includes some plausibility arguments, e.g., the dropping of "secular terms". Also $\langle v^2 \rangle$ has to be carefully defined. See [14] for the details.
[19] M. Lüscher, P. Weisz, J. High Energy Phys. 0109 (2001) 010, J. High Energy Phys. 0207 (2002) 049.
[20] Y. Burnier, H-T. Ding, O. Kaczmarek, A-L. Kruse, M. Laine, J. High Energy Phys. 11 (2017) 206.
[21] R.G. Edwards, U.M. Heller, T.R. Klassen, Nucl. Phys. B 517 (1998) 377.
[22] R. Sommer, Nucl. Phys. B 411 (1994) 839.
[23] C. Christensen, M. Laine, Phys. Lett. B 755 (2016) 316, arXiv:1601.01573.
[24] G.P. Lepage, P.B. Mackenzie, Phys. Rev. D 48 (1993) 2250.
[25] A. Francis, O. Kaczmarek, M. Laine, J. langelage, PoS LATTICE2011 (2011) 202, https://doi.org/10.22323/1.139.0202.
[26] B. Efron, SIAM Rev. 21 (1979) 460.
[27] Y. Burnier, M. Laine, J. Langelage, L. Mether, J. High Energy Phys. 08 (2010) 094.

[28] Note that the EE correlator at LO does not have a diffusion term; the leading order estimate for κ_E/T^3 comes from the EE correlator calculated at NLO.
[29] M. Laine, G.D. Moore, O. Philipsen, M. Tassler, J. High Energy Phys. 05 (2009) 014.
[30] The spectral function for the current density operator, $\rho_{JJ}(\omega)$, shows a diffusive peak. Here we are interested in a force-force correlator, eq. (2). Defining the force operator as $M\frac{dJ}{dt}$, one can argue [7] that in the static limit the peak structure of $\rho_{JJ}(\omega)$ leads to a smooth low-ω structure for $\rho_T(\omega)$. Such a smooth infrared structure for $\rho_T(\omega)$ is obtained in perturbation theory [7,27] as well as in classical lattice gauge theory [29]. Nonperturbative lattice correlators also support such a structure [9,11].
[31] M. Lüscher, J. High Energy Phys. 08 (2010) 071.
[32] S.Y.F. Liu, M. He, R. Rapp, Phys. Rev. C 99 (2019) 055201;
S.Y.F. Liu, R. Rapp, Eur. Phys. J. A 56 (2020) 44.
[33] O. Andreev, Mod. Phys. Lett. A 33 (2018) 1850041.
[34] ALICE Collaboration, J. High Energy Phys. 01 (2022) 174.
[35] R. Rapp, et al., Nucl. Phys. A 979 (2018) 21.
[36] S. Cao, et al., Phys. Rev. C 99 (2019) 054907.
[37] Y. Xu, J. Bernhard, S. Bass, M. Nahrgang, S. Cao, Phys. Rev. C 97 (2018) 014907.
[38] S.K. Das, F. Scardina, S. Plumari, V. Greco, Phys. Lett. B 747 (2015) 260.
[39] Here we have done a simple χ^2 analysis, treating the error band in Table 2 as a statistical 1σ band. The error band in the table is dominated by systematic errors. So while the fit does indicate that the data is inconsistent with a flat behavior with temperature, one should not attribute the standard 1σ interpretation to the error bars quoted for the fit parameters.
[40] P. Dierckx, Comput. Graph. Image Process. 20 (1982) 171.
[41] https://scipy.org.
[42] Y. Burnier, M. Laine, J. High Energy Phys. 11 (2012) 086.